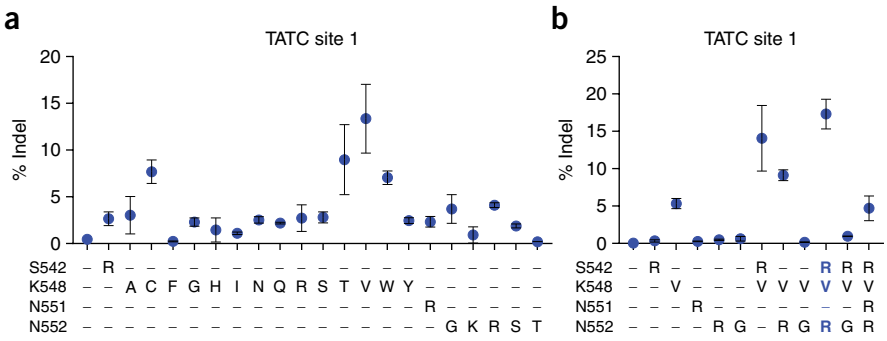

Supplementary Figure 1 Related to **Figure 2a**. Evaluation of (**a**) single amino acid mutations and (**b**) combination mutants to construct the AsCpf1 RVR variant, which is active at target sites with TATV PAMs. Dots show mean ± s.e.m. ($n = 2$).

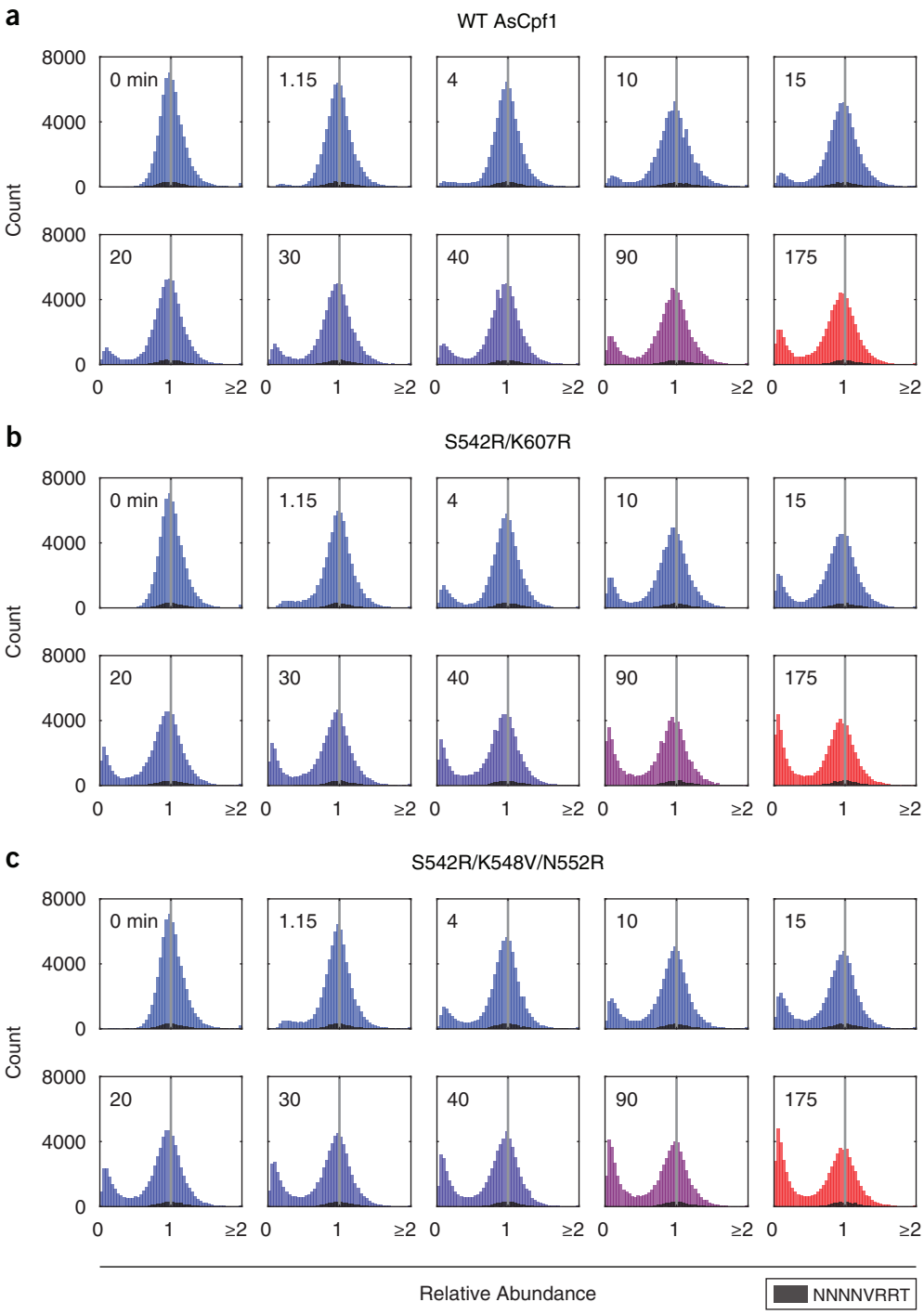

Supplementary Figure 2 Related to **Figure 2b-d**. Histograms of abundances of 4^8 PAMs (NNNNNNNN) at each *in vitro* cleavage time point for (**a**) WT AsCpf1, (**b**) S542R/K607R, and (**c**) S542R/K548V/N552R. The color of each histogram represents elapsed time. NNNNVRRT sequences, which were used to center the histograms, are shown in black.

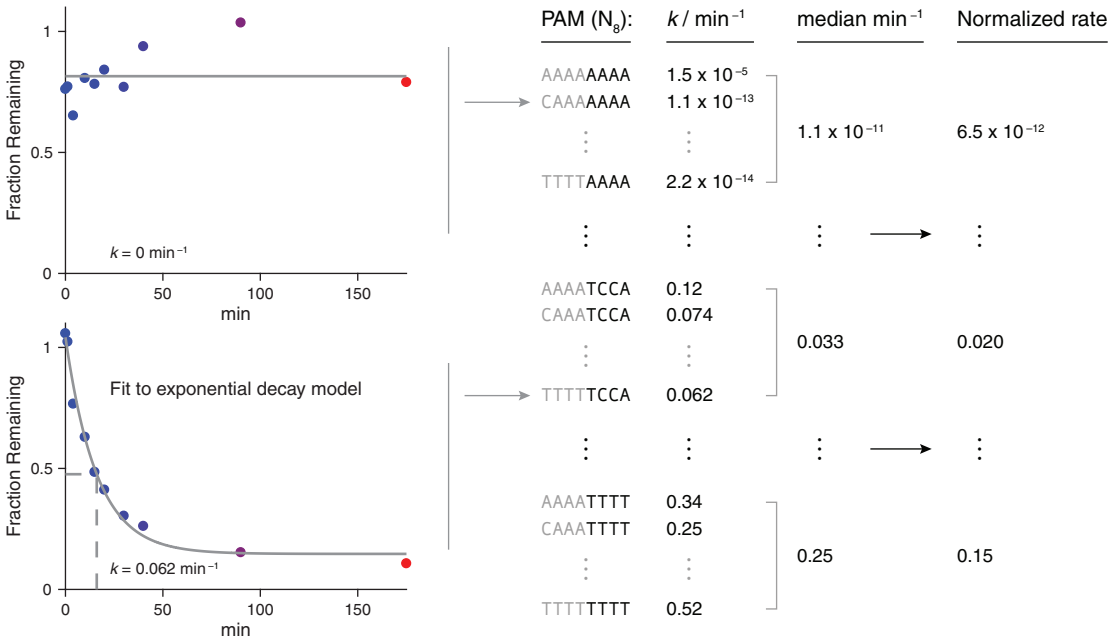

Supplementary Figure 3 Data processing pipeline for the *in vitro* cleavage assay used for **Figure 2d**.

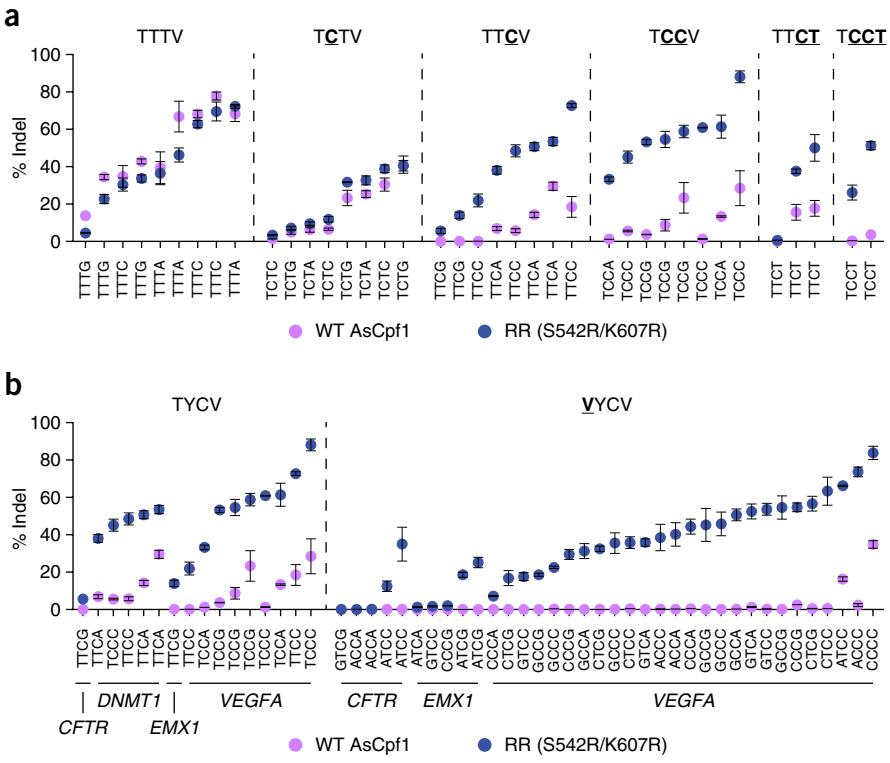

Supplementary Figure 4 (**a**) Comparison of the activity of WT AsCpf1 to the RR variant at target sites with cytosine-containing PAMs. (**b**) Activity of the RR variant at TYCV and VYCV sites (V = A, C, or G), demonstrating that the presence of a 5' T in the PAM sequence can be optional in many cases (*i.e.*, NYCV PAMs can be recognized). The data for TYCV sites is the same as that shown in (**a**). All indel percentages were measured in HEK293T cells. Dots show mean ± s.e.m. (n = 2-3).

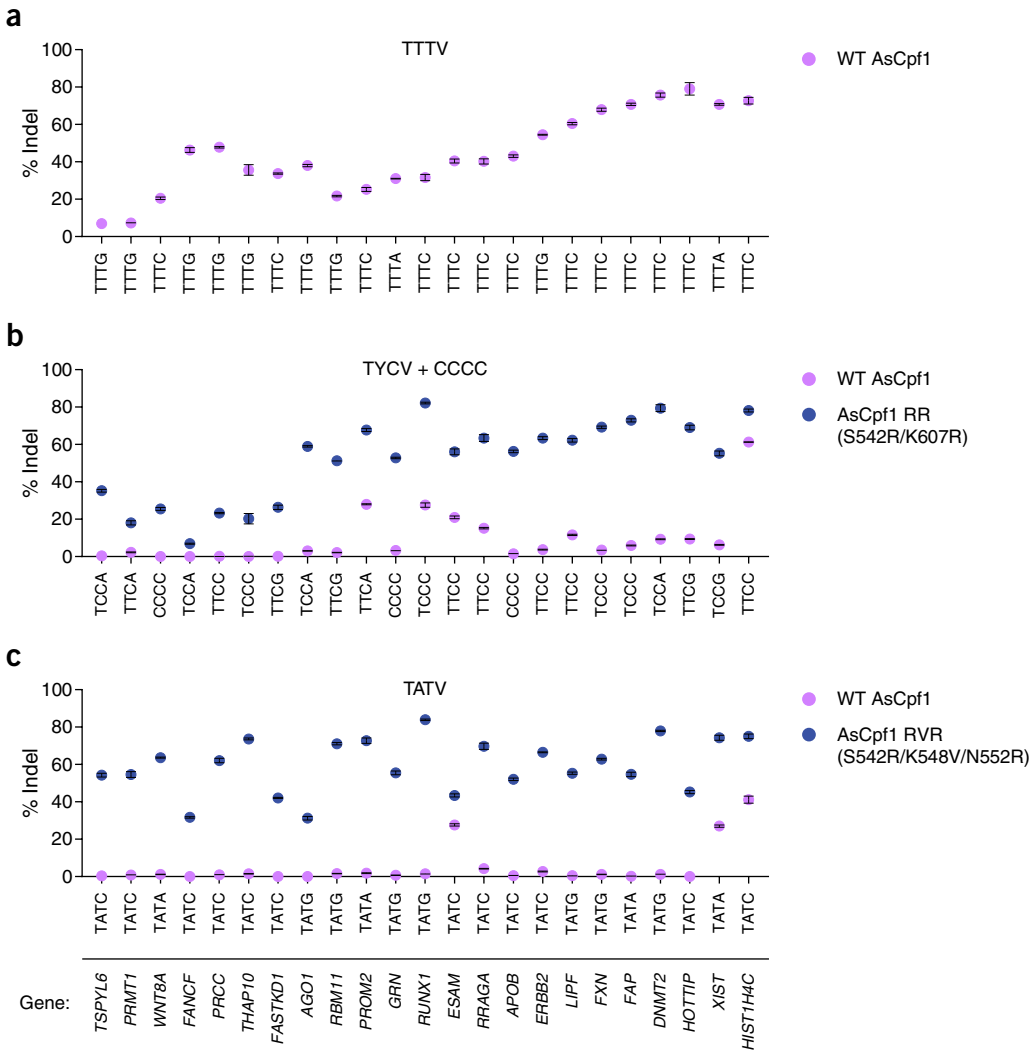

Supplementary Figure 5 Related to **Figure 2e**. Activity of (**a**) WT AsCpf1, (**b**) the RR variant, and (**c**) the RVR variant at target sites with highly active PAMs in HEK293T cells. Dots show mean ± s.e.m. ($n = 3$). **Figure 2e** shows these data in aggregate. For the AsCpf1 RR variant, the three CCCC sites are not included in **Figure 2e**.

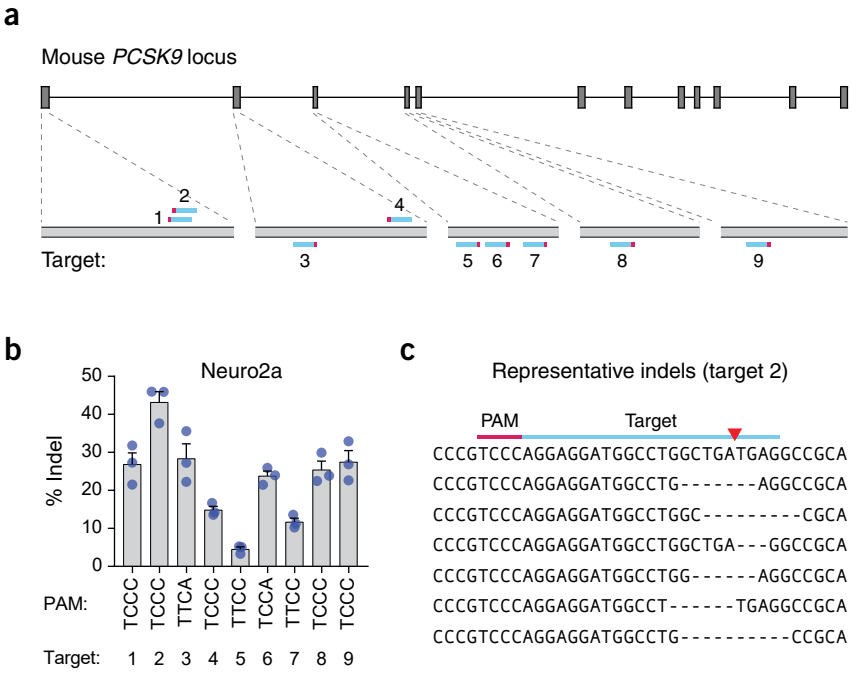

Supplementary Figure 6 Editing efficiency of the AsCpf1 RR variant at TYCV sites in mouse Neuro2a cells. (**a**) Diagram of the mouse *PCSK9* locus. Gray boxes represent coding sequences. (**b**) Indel percentages produced by the RR variant at *PCSK9* target sites with TYCV PAMs. Bars show mean ± s.e.m. ($n = 3$). (**c**) Representative indels at the target site (#2) with the highest editing efficiency. The red triangle represents the putative cleavage site on the top strand.

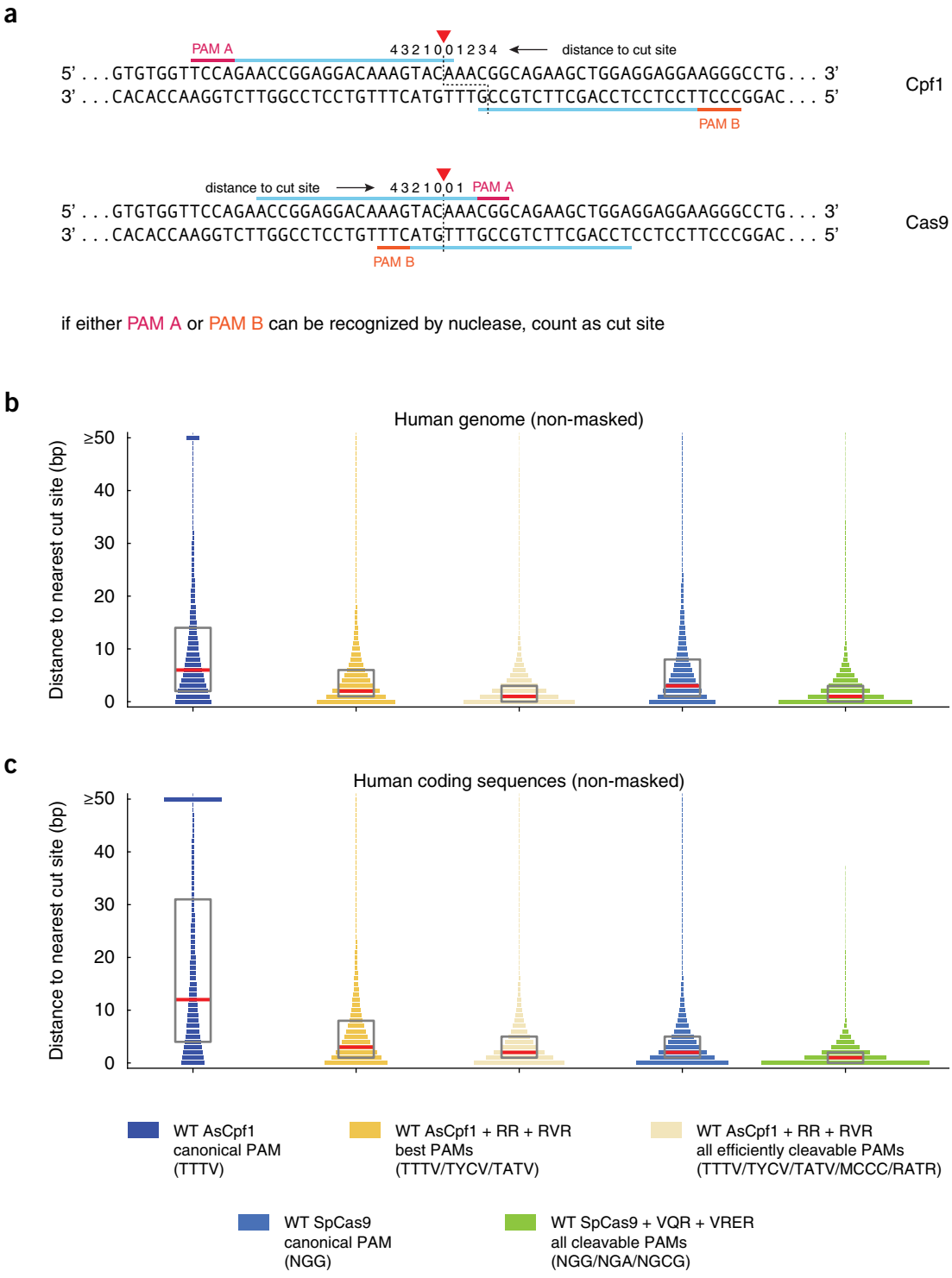

Supplementary Figure 7 Related to **Figure 2f**. (**a**) Definition of targeting range for Cpf1 and Cas9. Comparison of the targeting range of Cpf1 (+RR and RVR variants) to Cas9 (+VQR and VRER variants) in (**b**) the human genome and (**c**) coding sequences. Plots show the probability mass function of the distance (in base pairs) to the nearest cleavage site. The boxplots indicate median and interquartile range. Genomic regions that contain Ns or masked repeats were ignored in this analysis.

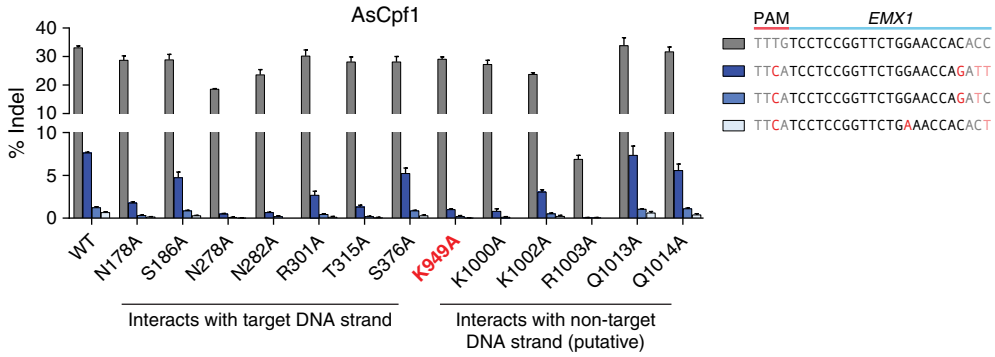

Supplementary Figure 8 Related to **Figure 3c**. Specificity mutagenesis of AsCpf1. An alanine scan of residues with interactions or putative interactions with the DNA strands. Bars show mean ± s.e.m. (n = 2-3). K949A was selected as a candidate for enhancing the specificity of AsCpf1. Lys949 is part of the bridge helix.

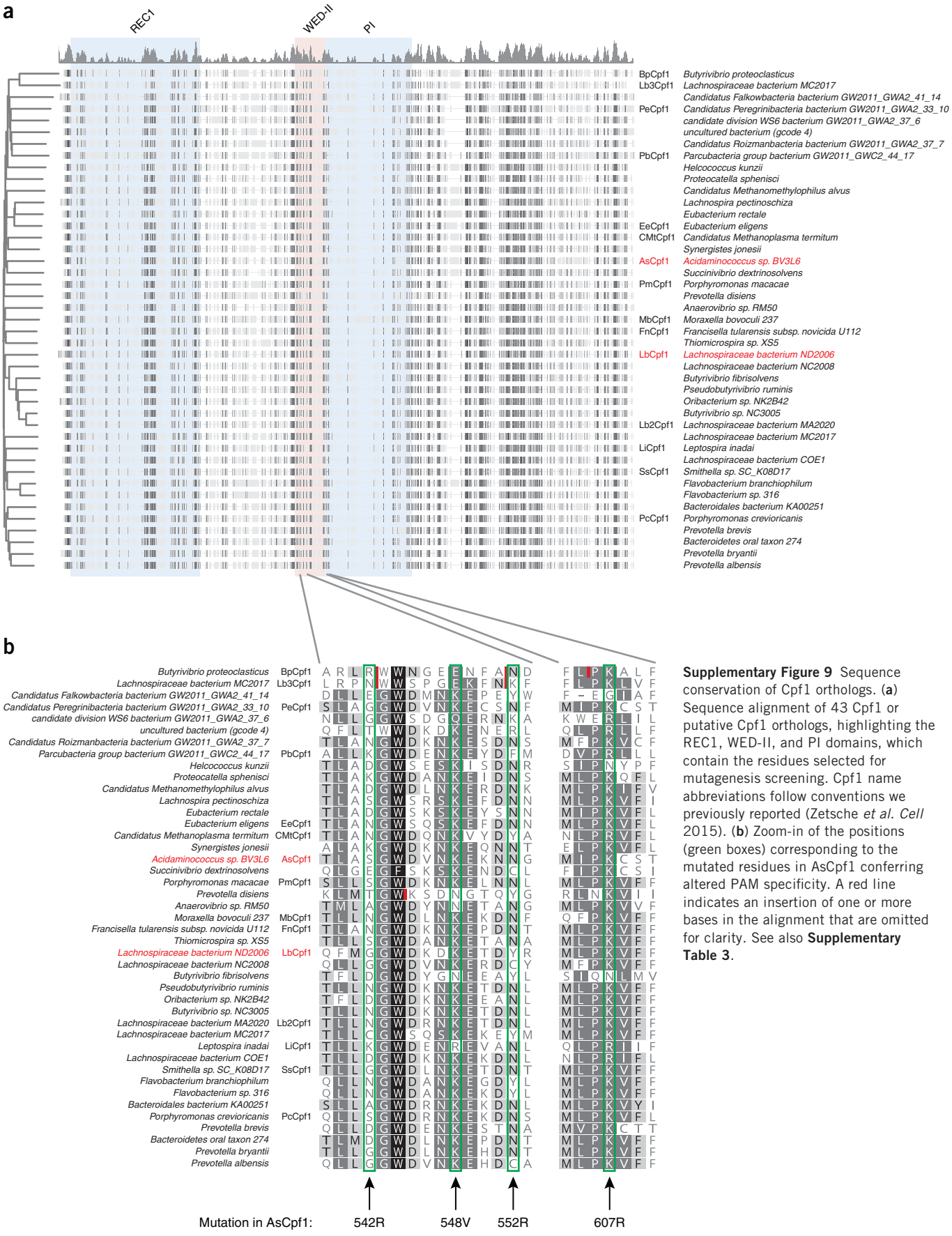

Supplementary Figure 9 Sequence conservation of Cpf1 orthologs. (**a**) Sequence alignment of 43 Cpf1 or putative Cpf1 orthologs, highlighting the REC1, WED-II, and PI domains, which contain the residues selected for mutagenesis screening. Cpf1 name abbreviations follow conventions we previously reported (Zetsche *et al. Cell* 2015). (**b**) Zoom-in of the positions (green boxes) corresponding to the mutated residues in AsCpf1 conferring altered PAM specificity. A red line indicates an insertion of one or more bases in the alignment that are omitted for clarity. See also **Supplementary Table 3**.

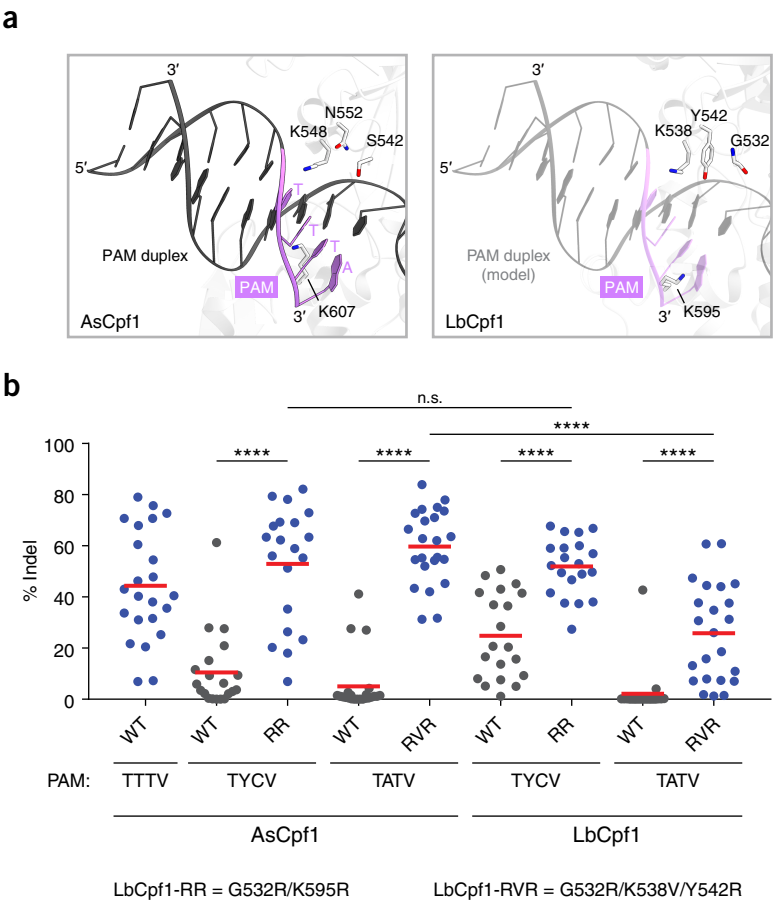

Supplementary Figure 10 Engineering the PAM recognition of LbCpf1. (**a**) Crystal structures of AsCpf1 (PBD ID: 5B43) and LbCpf1 (PDB ID: 5ID6), highlighting the corresponding residues mutated to alter PAM specificity. The PAM duplex shown for LbCpf1 is a model. (**b**) Activity of LbCpf1 G532R/K595R and G532R/K538V/Y542R at TYCV and TATV sites, respectively, in HEK293T cells. Each point represents the mean of three replicates, and the red lines indicate the overall means within each group. The data for AsCpf1 also appears in **Figure 2e**. n.s. $p > 0.05$ (Mann-Whitney); ****$p < 0.0001$ (Wilcoxon signed-rank).

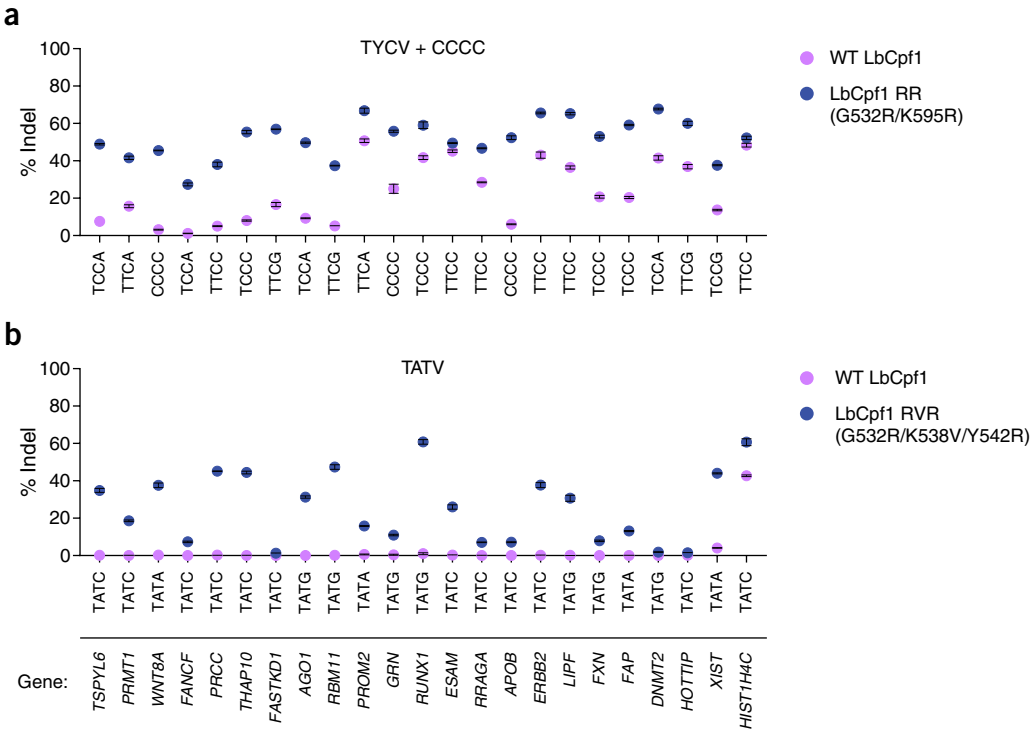

Supplementary Figure 11 Related to **Supplementary Figure 10b**. Activity of the (**a**) LbCpf1 RR variant and (**b**) LbCpf1 RVR variant at target sites with preferred PAMs in HEK293T cells. Dots show mean ± s.e.m. (n = 3). **Supplementary Figure 10b** shows these data in aggregate. The target sites are the same as those shown in **Supplementary Figure 5b-c**. For the RR variant, the three CCCC sites are not included in **Supplementary Figure 10b**.